Materials & Design 258 (2025) 114699

Contents lists available at ScienceDirect

Materials & Design

journal homepage: www.elsevier.com/locate/matdes

Exoskeletons of mud crabs, *Scylla serrata*, of different sizes: Body weight, surface morphology, internal tissue structure, and mechanical resistance

Tadanobu Inoue [a,*], Takahiro Yoshihama [b]

[a] National Institute for Materials Science, 1-2-1, Sengen, Tsukuba 305-0047, Japan
[b] Kanizo, 1381-6 Sawada, Irabu Island, Miyakojima, Okinawa 906-0507, Japan

ARTICLE INFO

Keywords:
Crustacean cuticle
Bimodal bulge structure
Protection
Structure-property relations
Biomineralization

ABSTRACT

Few studies have simultaneously examined shell size and changes in the surface and interior of the exoskeleton across a wide range of body weights in mud crabs. This study first analyzed the relationship between the sex, weight, and shell size of 131 mud crabs caught in Okinawa, and compared the findings with data from seven regions. Next, using laser microscopy and nanoindentation, the study examined how surface morphology, internal structure, exoskeleton thickness, hardness, and Young's modulus change with body weight (*BW*) in 18 male crabs, weighing 249 g to 1920 g. The growth coefficients of mud crabs in Okinawa were 3.52 for males and 2.91 for females, and these values were the largest among those reported so far in various countries. The exoskeleton surface in mud crabs consisted of a bimodal bulge structure with a large bulge 264.5 μm in diameter and a small bulge 100 μm in diameter. Such surface morphology and thickness of the hard exocuticle of 150 μm were independent of *BW*. On the other hand, the endocuticle thickness increased with *BW*. Even if the exoskeleton feels hard, the endocuticle may be thin because it is not fully developed by the effect of molting.

1. Introduction

The emergence of new material-processing technologies, such as 3D printing, has enabled the fabrication of materials with complex hierarchical structure as found in living organisms [1–4]. Consequently, understanding the complex biological structures is becoming more important, and research is underway to elucidate the microstructure, morphology, and characteristics of various organisms, with the goal of enhancing the properties and functions of materials [3–8].

The exoskeleton of arthropods has a robust internal tissue structure based on a twisted plywood–pattern structure (TPS) [9] to protect the body from enemy attack and desiccation. The TPS, usually referred to as the Bouligand structure, is formed by a regular stacking of bundles of chitin fiber wrapped with protein [9–13]. The stacking height (S_h) of this pattern, exoskeleton thickness, and mechanical properties varies depending on the organism and body part [14–26]. The mud crab, *Scylla serrata*, classified as a crab of the genus *Scylla* in the family Portunidae, is a large crab found in the tropical and subtropical regions of the Indo-Pacific [27–32]. It is also an important edible species [33]. One of the characteristics of the mud crab is its robust exoskeleton and huge claws [13,24,32,34,35], as shown in Fig. S1 of the Supporting Materials. The carapace is disc-shaped, with six sharp saw-like teeth on the front and nine on each side of the carapace from the eye (Fig. S1(a)). The surface of the exoskeleton is a mottled deep blue to brown, clean and shiny. The shape of the abdomen is a thin triangular apron for males (Fig. S1(b)), while that of females is wider [30], as shown in Fig. S2 of the Supporting Materials. On the pinching side of the claws, there is a row of white tooth-like denticles, which are larger at the base of the claw finger and get smaller towards the tip (Fig. S1(a,c)) [24,32,34]. A previous study [36] has shown that the mud crab's mottled, deep-blue exoskeleton surface has fine bulges, as shown in Fig. S1(d). Such a bulge in the exoskeleton surface of the crab has also been observed in the exoskeleton surface of the brown crab [11], the snapping shrimp [22], the Atlantic blue crab [21], and the Mediterranean green crab [21]. The apex of the bulge is connected to a tube that bundles many pore canals that penetrate the exoskeleton. Most of the inside of the exoskeleton is occupied by the endocuticle with a TPS, and the exocuticle with a fish scale-like structure exists directly below the surface between the bulges.

In material research, the biggest problem when using living organisms is the quality and quantity of the specimen. Characterization of the microstructure and the mechanical property is often based on only one specimen. In some literature, the weight, size, and sex of the specimen

* Corresponding author.
E-mail address: INOUE.Tadanobu@nims.go.jp (T. Inoue).

https://doi.org/10.1016/j.matdes.2025.114699
Received 13 May 2025; Received in revised form 29 August 2025; Accepted 4 September 2025
Available online 5 September 2025

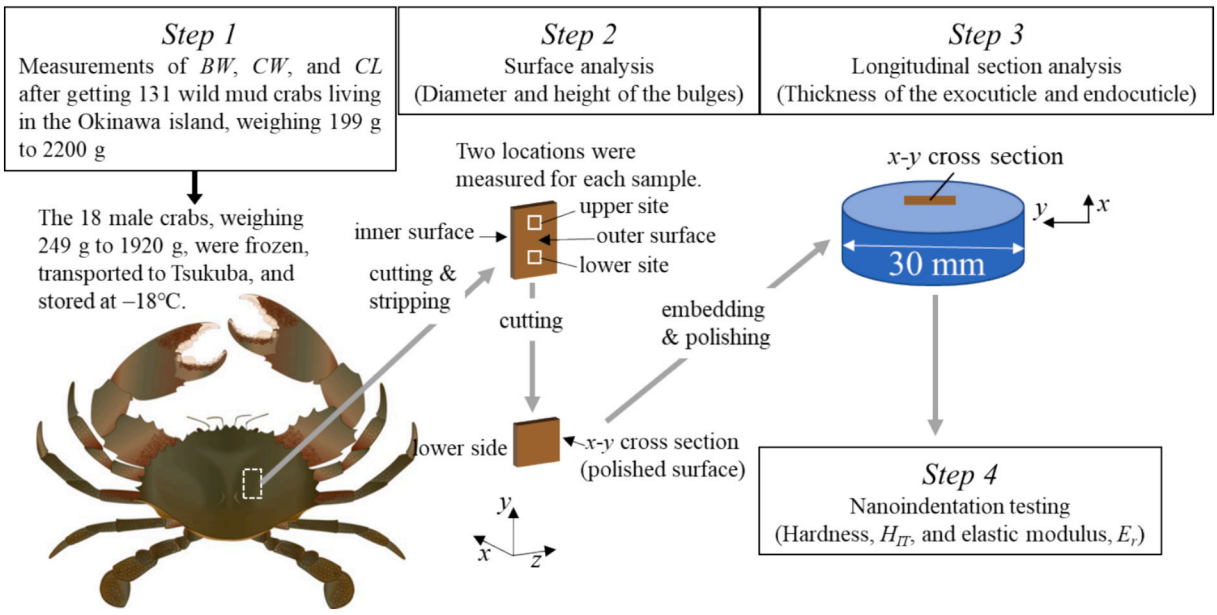

Fig. 1. Outline of this study.

are not specified. However, if the tissue structure, elemental composition, and hardness of the exoskeleton depend on the body size, sex, and individual sample (related to molting), such information is necessary for the outcome of the study. This oversight is likely due to lack of collaboration with biological experts. In order for the results to be universal, multiple biological specimens must be used. However, even if multiple biological specimens are collected, it is difficult to obtain specimens of the same weight and size. In addition, crustaceans molt. After molting, the exoskeleton is obviously soft, as it is called a soft shell, and the tissue and properties of the exoskeleton change with time after molting [37]. However, it is very difficult for material researchers to accurately determine the molting stage of wild crustaceans. Therefore, it is necessary to have biological experts determine the molting stage and then analyze and compare crab exoskeletons of various sizes using a materials science approach. Few studies have simultaneously examined shell size and changes in the surface and interior of the exoskeleton across a wide range of body weights in mud crabs.

In this study, we first systematically investigated the relationship between sex, weight, and shell size of the mud crab, which lives in Okinawa, weighs 199 to 2200 g, and has exoskeleton that has sufficiently hardened after molting. The results were compared with those obtained in other habitats (Indonesia, Bangladesh, Mozambique, India, and the northern Persian Gulf). We then used a laser microscope and nanoindentation to clarify the changes in shell surface morphology, internal structure, exoskeleton thickness, hardness, and Young's modulus against body weight (*BW*) in 18 male crabs, including the effects of molting.

2. Materials and methods

All 131 mud crabs were collected from the Okinawa Islands of Japan. When the sample is a wild mud crab, the exoskeleton has become sufficiently hard can be estimated based on the color of the carapace (from whitish to deep blue). According to the Fisheries fact sheet [33], the mud crab reaches sexual maturity at 18 to 24 months and matures with a carapace width (*CW*) of approximately 110 mm. It is said that the width of a mud crab's carapace reaches 100 mm in about a year. In another paper [31], crabs with *CW* over 100 mm were described as adult crabs. The growth of crabs is influenced by their habitat and staple food [30], but the mud crabs of $CW \geq 100$ mm can be considered adults. For example, since the crab shown in Fig. S1 is 169.6 mm in *CW* and 1442 g in *BW*, the crab sample is an adult crab estimated to be over 1.5 years old.

As illustrated in Fig. 1, this study proceeded in four steps. As *step* 1, the *BW* and carapace size (*CW* and a carapace length, *CL*) of all crabs were measured live. The size was precisely recorded using a digital caliper. In addition, male and female were judged based on the shape of the abdomen, as shown in Fig. S2. Only 18 male crabs of different weights (that we were able to obtain) were frozen and transported to Tsukuba for *step* 2. Before freezing the crabs, general anesthesia was applied by dipping the crab into cold ice water (approximately 0–4 °C) to minimize its suffering. The 18 test pieces were cut from the carapace using a microgrinder (Minimo ONE SERIES ver.3, MINITOR Co., LTD., Tokyo). At that time, the test pieces were extracted from a location that avoided the H-shaped depression in the center of the carapace seen in Fig. S1(a). As *step* 2, the diameters of the bulges on the exoskeleton surface were quantitaively measured using a 3D laser scanning microscope (VK-X200/210, Keyence Corporation, Osaka, Japan). Interestingly, the exoskeleton surface had a bimodal bulge structure with large and small bulges. In the images of each site, the diameters of 10 large bulges and 10 small bulges were measured and they were recorded as (average values ± standard deviation). Subsequently, all pieces were cut in half with a microgrinder. After drying the samples for more than 48 h, the 30 mm diameter mounting cup in which the samples were set was filled with epoxy (HERZOG Epo, Herzog Japan Co., LTD., Tokyo, Japan) and left to cure at 23 °C for 12 h. After that, each sample was ground with Grit400/600 grade SiC papers, polished with a 9, 3, and 1 μm diamond suspension, and finally polished with a 0.02 μm colloidal silica suspension. After polishing, cross-sectional images of the samples were taken with an OM to measure the exoskeleton thickness (*step* 3). In the images of each sample, the thicknesses of exocuticle and endocuticle layers at 10 locations were measured and summarized as (average values ± standard deviation). Finally, nanoindentation tests were conducted to obtain hardness and elastic modulus (*step* 4). The testing was conducted at 23 °C using a dynamic ultra-micro hardness tester, DUH-211S (SHIMADZU, Kyoto, Japan) with a Berkovich diamond indenter. The loading curve consisted of a loading rate of 1.4632 mN/s, holding for 5 s at the maximum load of 5 mN, and then a 5 s unloading time. Since the apex of the surface bulge is connected to a thick bundle that penetrates the exoskeleton, these areas were avoided as measurement sites. That is, tests were done from the exocuticle in the valley part of the surface through the endocuticle. The tests were performed on two

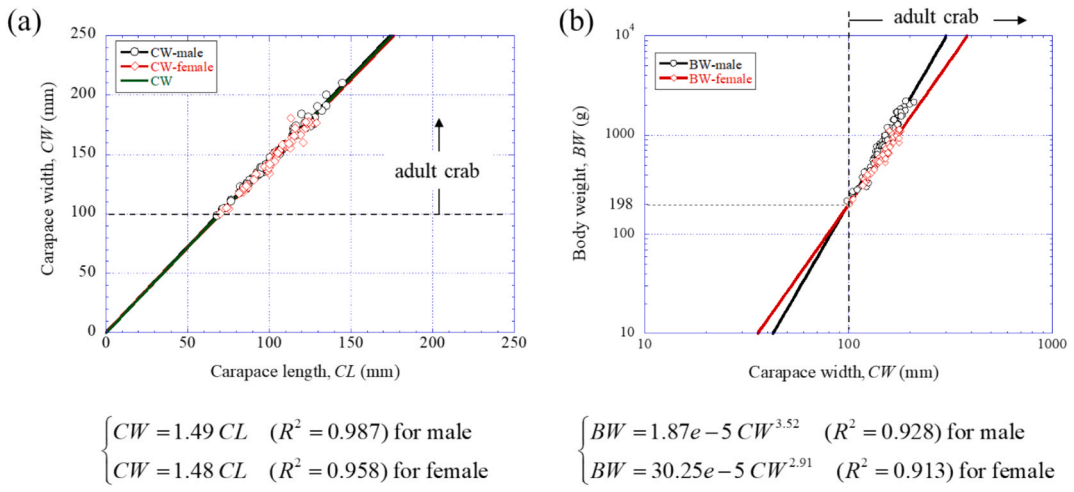

Fig. 2. Relationship between (a) carapace length (*CL*) and carapace width (*CW*) and (b) *CW* and body weight (*BW*) for 79 male mud crabs and 52 female mud crabs.

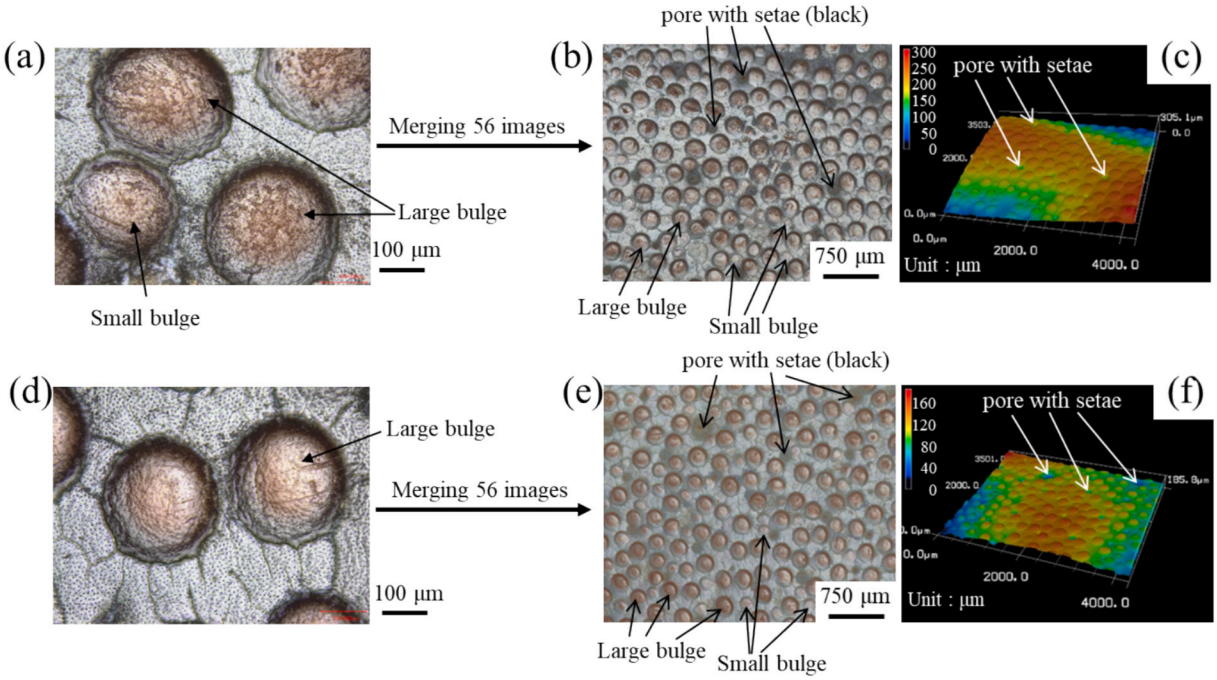

Fig. 3. The surface morphology of the (a–c) upper site and (d–f) lower site of the carapace of a 410 g mud crab. (a,d) Laser scanning microscope image, (b,e) merged scanning microscope image, and (c,f) 3D color map showing bulges.

parallel lines 100 μm apart for each sample and at an interval of 25 or 50 μm from an outer surface to an inner surface. The hardness (H_{IT}) and reduced elastic modulus (E_r) were analyzed by the Oliver–Pharr method employed in biological studies.

3. Results

3.1. Carapace size and body weight

Fig. 2 shows the relationship between *CL* and *CW* and *CW* and *BW* for males (79 crabs) and females (52 crabs). Three large mud crabs (2038 g, 2138 g, and 2200 g) in the 2 kg class were caught in Okinawa—all males—and the maximum shell size was 210 mm *CW* and 145 mm *CL* [35]. The *CW*–*CL* relationship shown in Fig. 2(a) is shown as $CW = 1.49 \times CL$ ($R^2 = 0.987$) for males and $CW = 1.48 \times CL$ ($R^2 = 0.958$) for females. In other words, the slope, *c*, is almost the same and there is no difference in carapace size between the sexes. This result is consistent with that of 165 mud crabs examined in the Persian Gulf ($c = 1.45$ for males and $c = 1.46$ for females) [28]. The *CW*–*BW* relationship is estimated as $BW = a\,CW^{b}$, where *a* is the condition factor, and the exponent *b* is the growth coefficient [28,30]. The *BW*–*CW* relationship seen in Fig. 2(b) shows that males are heavier than females, even with the same carapace size.

3.2. Morphology of the exoskeleton surface

Fig. 3 shows the result of surface analysis of the carapace exoskeleton for a 410 g mud crab. The exoskeleton surface consists of large bulge, small bulge, and pore with setae, as shown in Fig. 3(a,b,d,e). The 3D maps shown in Fig. 3(c,f) clearly show that there is unevenness on the exoskeleton surface. From the merged images in Fig. 3(b,e) and observation results, the proportion of large bulges was higher than that of small bulges. The diameters of the large and small bulges were 269.6 ± 11.0 μm and 95.1 ± 14.9 μm for the upper site, and they were 251.3 ±

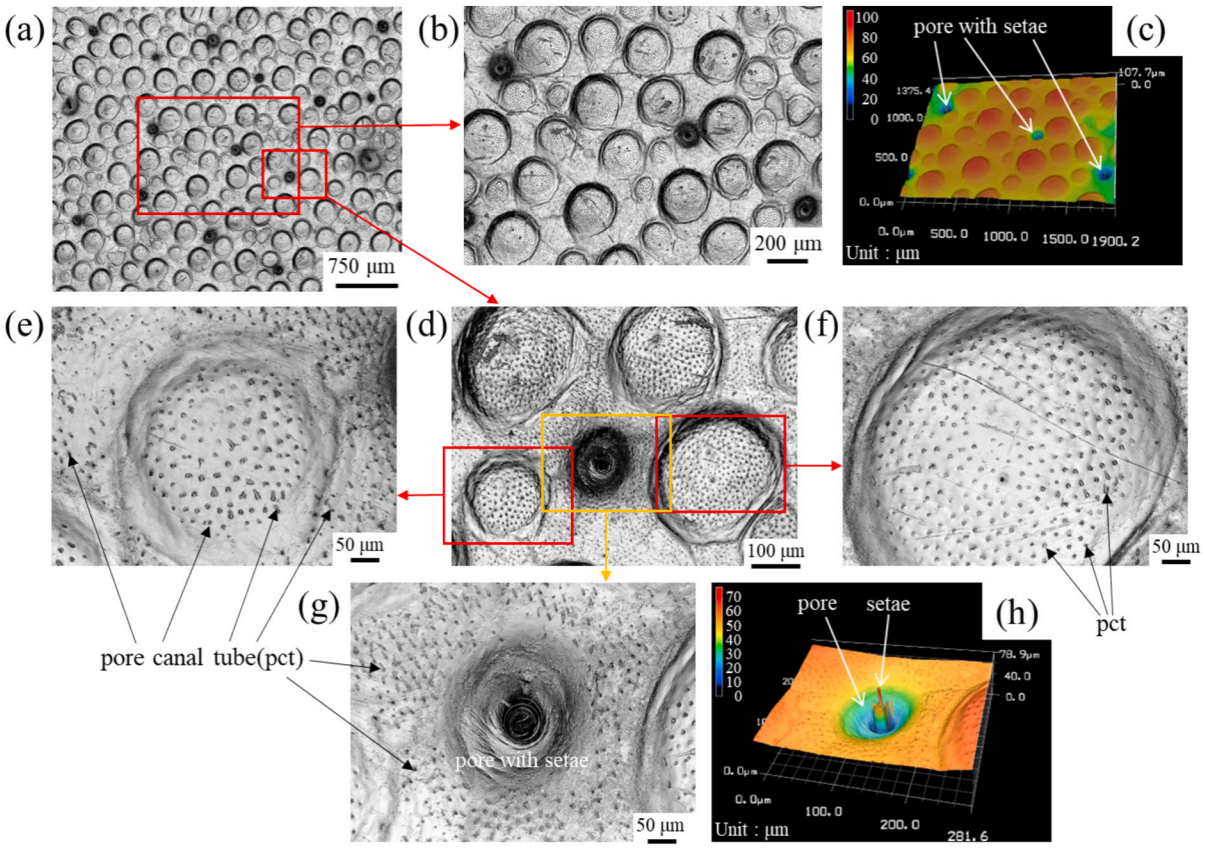

Fig. 4. The surface morphology of the upper site on the carapace of a 985 g mud crab. (a) Laser scanning microscope image, (b) enlarged view of (a), and (c) its 3D color map. (d) Enlarged view of (a), enlarged views of (e) small bulge and (f) large bulge in (d), (g) enlarged view of pore with setae in (d), and (h) its 3D color map.

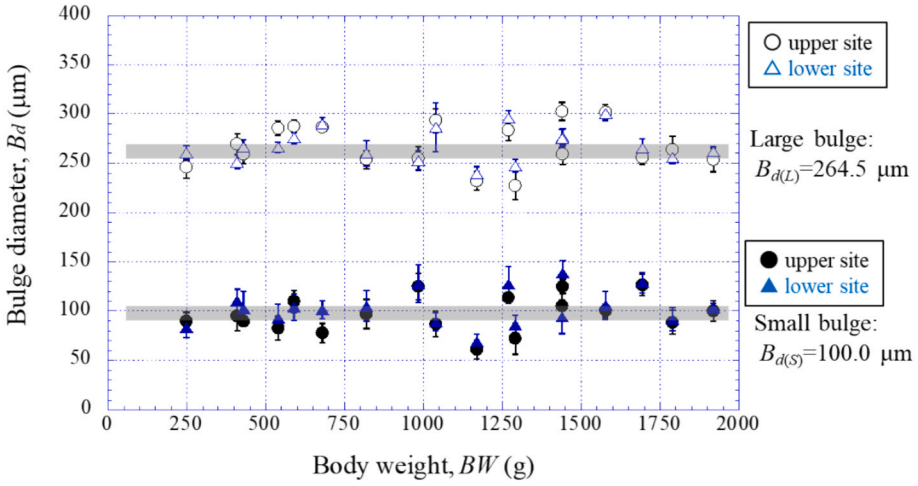

Fig. 5. Relationship between body weight (*BW*) and bulge diameter (B_d) in mud crabs. Here, error bars represent standard deviations.

7.1 μm and 110.7 ± 11.4 μm for the lower site, respectively (see Fig. S3 of the Supporting Materials for details). Some black areas seen in Fig. 3 (b,e) are the pores with setae, which are displayed as large concave areas (blue to green) on the 3D maps in Fig. 3(c,f). Fig. 4 shows the results for a 985 g mud crab, which has more than twice the body weight of the crab shown in Fig. 3. The exoskeleton surface is a bimodal bulge structure, with the diameters of the large and small bulges being 254.7 ± 12.2 μm and 124.9 ± 13.5 μm for the upper site, respectively (Fig. S4 of the Supporting Materials). The setae were more clearly visible (Fig. 4(a,b,d, g,h)), and ultrafine pores and tubes corresponding to pore canals can be observed on the exoskeleton surface (Fig. 4(d–g)). A comparison of the exoskeleton surfaces of mud crabs weighing from 249 g to 1790 g is shown in Figs. S5 and S6 of the Supporting Materials, including quantitative analyses of the diameters of the large and small bulges. Since the samples are wild crabs and they were frozen, transported, thawed, and dried, individual differences in surface texture were seen. For example, an 820 g crab has relatively small scratches (Fig. S5(e)), while a 1790 g crab has large, deep scratches (Fig. S5(k)). Ultrafine pores (black) corresponding to pore canals are clearly observed on the surface of the bulges of 249 g, 680 g, 1170 g, 1292 g, and 1790 g crabs, but not on the

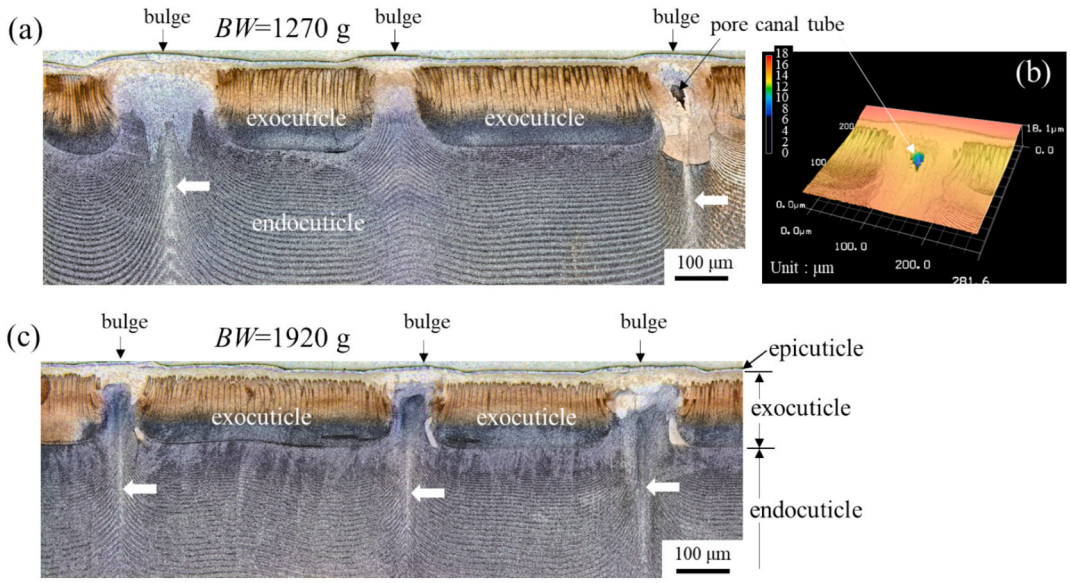

Fig. 6. (a) Optical micrograph (OM) near the outer surface in the *x-y* cross section of a 1270 g mud crab and (b) 3D color near the pore canal tube, and (c) OM of a 1920 g mud crab. In (a) and (c), the white arrows denote the traces of pore canal tubes observed on the polished surface.

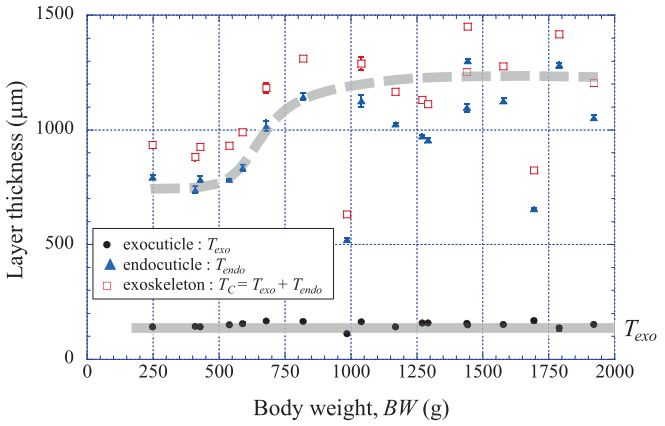

Fig. 7. Variations of exocuticle thickness (T_{exo}), endocuticle thickness (T_{endo}), and exoskeleton thickness (T_C) with *BW* in mud crabs. Here, error bars represent standard deviations.

surfaces of the 410 g (Fig. 3(a,d)) and 820 g crabs.

Fig. 5 shows the relationship between *BW* and bulge diameters. The diameter of the larger bulge, $B_{d(L)}$, was 227–302 μm (average 264.5 μm), and that of the smaller bulge, $B_{d(S)}$, was 61–139 μm (average 100.0 μm), indicating that these diameters remain constant as *BW* increases.

3.3. Exoskeleton thickness

Fig. 6 shows the optical micrographs near the surface in the exoskeleton cross section of 1270 g and 1920 g crabs. For the 1270 g crab, a 3D color map near the cross section of a clearly observed pore canal tube was also presented. As shown in Fig. 6 and Fig. S7 of the Supporting Materials, observed in detail by SEM, the hard exocuticle of the mud crab consists of a fish scale–like structure and exists directly below the surface between the bulges [36]. The endocuticle is adjacent to the exocuticle and consists of a TPS. The intermediate layer, which is the boundary between two layers, can be seen clearly by cracking due to drying during SEM observation for several hours under vacuum (Fig. S7) and can be identified simply on the polished surface by an OM (Fig. 6(a, c)). Fig. S8(a,b) of the Supporting Materials shows OMs of the *x–y* cross section of 410 g and 1790 g mud crabs, the thickness measurement data at 10 locations, and the thickness results of each layer. For comparison, the results of two crabs (985 g and 1694 g), which had extremely thin exoskeletons, are also shown in Fig. S8(c,d). The exocuticle thickness (T_{exo}) was 142.8 ± 4.5 μm for the 410 g crab and 134.9 ± 10.2 μm for the 1790 g crab. The endocuticle thickness (T_{endo}) was 739.3 ± 15.0 μm for the 410 g crab and 1282.4 ± 10.6 μm for the 1790 g crab. That is, the T_{exo} is almost the same, but the T_{endo} was significantly different. In Figs. S8(c,d), the T_{exo} was 109.9 ± 3.4 μm for the 985 g crab and 167.4 ± 8.6 μm for the 1694 g crab; considering the previous two crabs, only the exocuticle of the 985 g crab seems to be slightly thinner. The T_{endo} was 521.3 ± 6.3 μm for the 985 g crab and 655.4 ± 5.1 μm for the 1694 g crab, and the T_{endo} differs with *BW*.

Fig. 7 shows variations of T_{exo}, T_{endo}, and exoskeleton thickness (T_C) against *BW*, where $T_C = T_{exo} + T_{endo}$. Although only the 985 g crab was low at $T_{exo} \approx 110$ μm, the exocuticle layers in the other crabs were constant at $T_{exo} \approx 150$ μm regardless of *BW*. On the other hand, the thickness of the endocuticle layer varied considerably with *BW*. The T_{endo} was approximately 750 μm when *BW* was 600 g or less and then increased with *BW*. When the *BW* exceeds 1000 g, the T_{endo} becomes 1200 μm, but there is large variability. In all data, the T_{endo} of the 985 g and 1694 g crabs was clearly lower than that of the other crabs.

3.4. Mechanical properties

Fig. 8(a,b) shows the distribution of the H_{IT} and E_r at distance *x* from the outer surface for the 410 g and 1790 g crabs. For comparison, the results of two crabs (985 g and 1694 g) that had thin endocuticles are shown in Fig. 8(c,d). The results for all specimens are shown in Fig. S9 of the Supporting Materials. In Fig. 8 (a,b), the H_{IT} and E_r decrease from the outer surface to the inside, showing a minimum value in the intermediate layer, and then becoming almost constant when *x* exceeds 200 μm. Since the region from the outer surface, which corresponds to the exocuticle, to 150 μm deep from Fig. 7, is a fish scale–like structure consisting of dense (hard) and coarse (soft) areas [36], the variation in mechanical properties in this region is large. In addition, the properties drop sharply from the surface to the intermediate layer. Although there is some variability in the endocuticle of a TPS, the values are relatively constant at $H_{IT} = 0.25$–0.45 GPa and $E_r = 10$–15 GPa. The properties of the two crabs with thin endocuticles shown in Fig. 8(c,d) also show similar results. However, the properties near the outer surface of the exocuticle are obviously lower than those shown in Fig. 8(a,b), while the

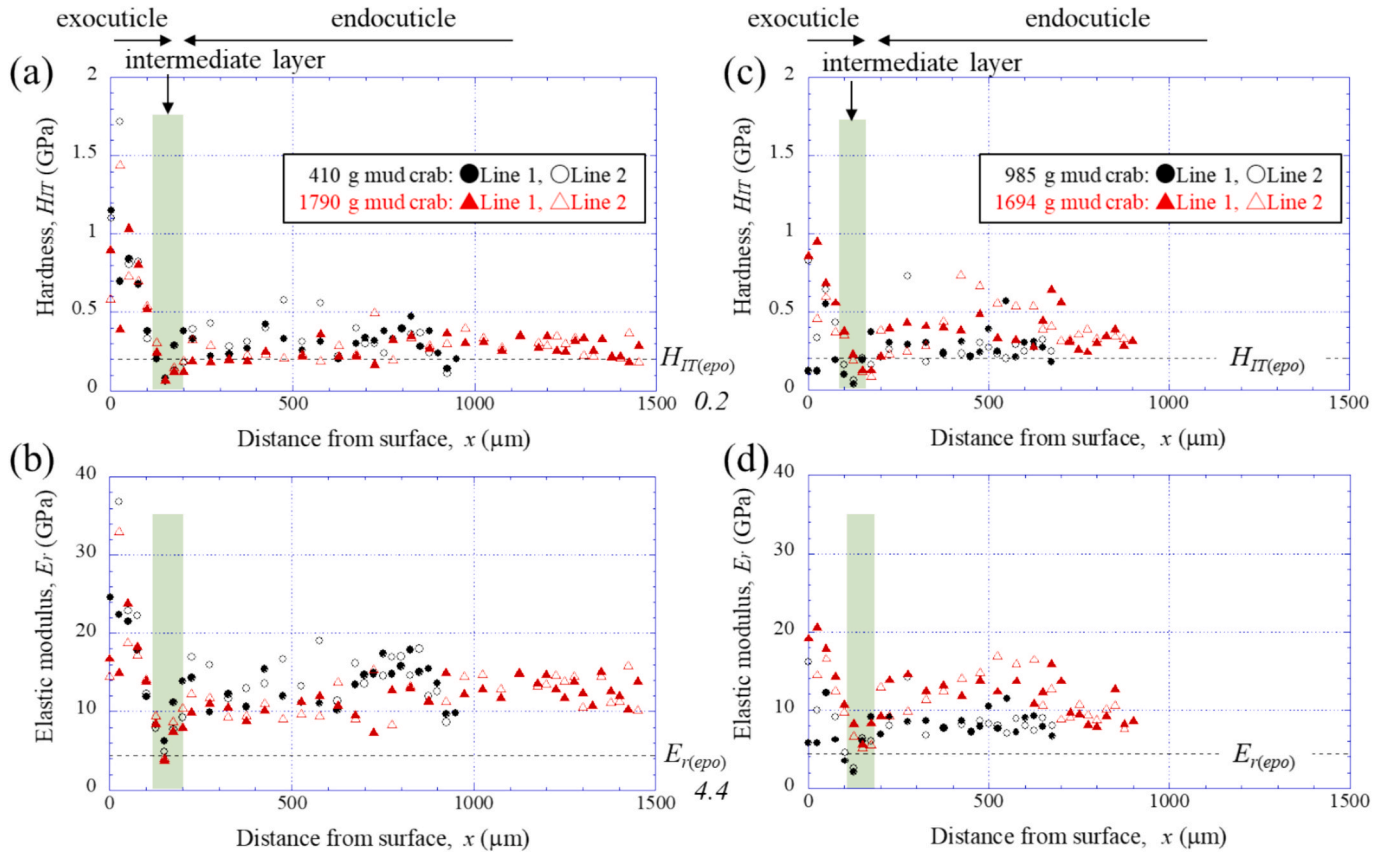

Fig. 8. Distributions of (a) hardness (H_{IT}) and (b) elastic modulus (E_r) with distance from the outer surface, x, on Line L1 and L2 in the carapace cross sections of 410 g and 1790 g crabs. The results of (c) H_{IT} and (d) E_r for 985 and 1694 g crabs with thin exoskeletons. Here, $H_{IT(epo)}$ and $E_{r(epo)}$ denote the hardness and elastic modulus, respectively, of the cold epoxy resin used as the embedded resin.

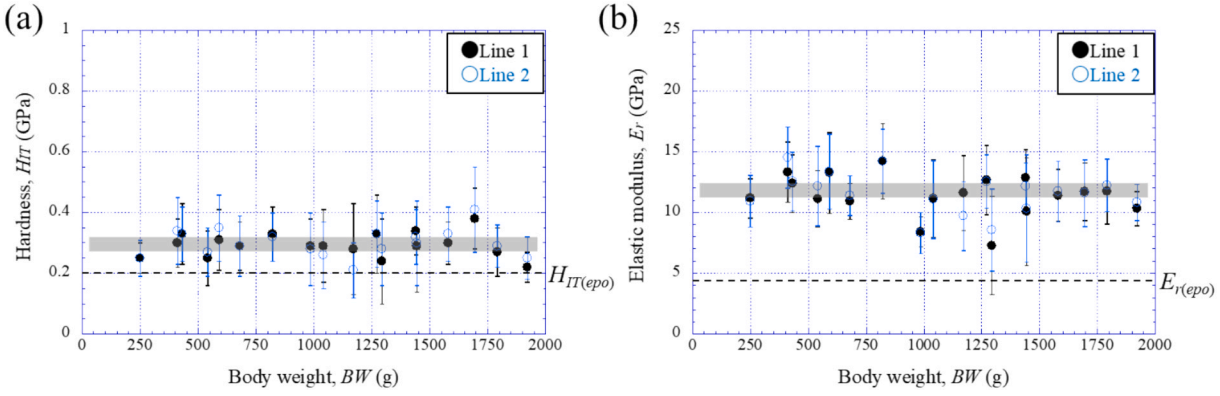

Fig. 9. Relationship between (a) $H_{IT(endo)}$ and BW and (b) $E_{r\ (endo)}$ and BW for the endocuticle layer (over x = 225 μm) in mud crab carapaces.

properties of the endocuticle appear to be slightly lower. In particular, the properties of the 985 g crab are low. In all crab data shown in Fig. S9, the mechanical properties showed a trend similar to the results shown in Fig. 8. Fig. 9 shows the variations of the $H_{IT(endo)}$ and $E_{r(endo)}$ with BW in the endocuticle layer. Here, the $H_{IT(endo)}$ and $E_{r(endo)}$ denote the average values of the H_{IT} and E_r, including their standard deviation in the region over x = 225 μm. It can be seen that the $H_{IT(endo)}$ and $E_{r(endo)}$ are independent of BW, $H_{IT(endo)} \approx 0.3$ GPa and $E_{r(endo)} \approx 12.0$ GPa.

4. Discussion

4.1. Growth

As seen in Fig. 2, males and females have similar shell sizes, but their growth rates differed. One reason for this is that, as in other brachyuran crab species [38], the claws of adult male mud crabs are larger than those of the same-sized female [27]. As can be seen from Fig. S2, although they do not have exactly the same BW, the claws of the males are larger and thicker than those of the females. The growth coefficients (the b-values) of mud crabs collected in Okinawa, Japan, were 3.52 for males and 2.91 for females, as shown in Fig. 2(b). These values are the largest among those collected, investigated, and reported so far in

Table 1
Comparison of the growth coefficient of the mud crab in different locations.

Location	Sex	*b*-value	Reference
Okinawa Island, Japan	male female	3.52 2.91	Present study
Northern Presian Gulf, Iran	male female	3.43 2.97	[28] H.Khaksari et al. (2023)
Chilika Lagoon, India	male female	3.22 2.75	[29] A.Mohapatra et al. (2010)
Bulungan District, Indonesia	male female	3.10 2.40	[30] B.Widigdo et al. (2017)
Kabupaten Subang, Indonesia	male female	3.16–3.20 2.26–2.52	[39] A.A.Kumalah et al. (2017)
Inhace Island, Mozambique	male female	3.02 2.43	[31] S.Toivio (2015)
Khulna region, Bangladesh	male female	3.06 1.89	[40] M.Y.Ali et al. (2004)
Northwestern Gulf, Oman	male female	3.48 2.52	[41] R.Savari et al. (2013)
Cochin Estuary, Southwest coast of India	male female	3.27 2.86	[42] K.A.Aneesa et al. (2025)

various countries. Table 1 summarizes the results of the *b*-values investigated at various locations. The difference in the *b*-values with respect to the length–weight relationships in mud crab might be due to changes in aquatic physiology, the amount and quality of food available in the environmental conditions, the time of sampling, and also in relation to the area under investigation [28]. Even for crabs living in the same place, the *b*-value is likely to change due to changes in the natural environment. The growth of crabs varies greatly depending on the habitat (water, food, etc.), and the current habitat of the Okinawa Islands is considered to be favorable for mud crab growth.

4.2. Surface morphology

As shown in Fig. 5, the exoskeleton surface consisted of a bimodal bulge structure with a large bulge 264.5 μm in diameter and a small bulge 100 μm in diameter. The diameter of these bulges remained constant as *BW* increased. This means that the bulge size on the exoskeleton surface is independent of body size. Usually, the scales that cover a fish's surface grow larger as its body grows [43,44]. For example, in goldfish, *Carassius auratus*, it is known that there is a linear relationship between the length of the scale radius and body length [43]. Based on the proportional relationship between fish length and the radius of the scales, it has been shown that the growth history, age, and body length of an individual fish can be estimated from the scale annuli [44–49]. On the other hand, in cartilaginous fishes such as sharks and rays, since new scales, known as "placoid scales", are added to the skin to adapt to the increased size of the body, the size of scales does not increase with the growth. In other words, the size of the scales and the density of the scales on the body surface remain constant regardless of body size. That is, the presence of the bulge on the exoskeleton surface of the mud crab is the same as that of the placoid scales. The fine bulges seen only on the mottled, deep-blue surface of the mud crab's exoskeleton allow it to mechanically disperse force, functionally disperse light, and achieve low adhesion [36]. For mud crabs, the fine bulges on the surface and the presence of the many pore canal tubes that penetrate those bulge peaks are important for maintaining a clean and strong carapace. A bimodal bulge structure with two diameters may be biologically, mechanically, and functionally superior to a uniform bulge structure. The two diameters (260.5 μm and 100.0 μm) may be the most suitable sizes for the carapace of adult mud crabs. Interestingly, these bimodal bulges were not seen on the tips of the sharp protrusions on the front and both sides of the disc-shaped carapace (see Fig. S10 of the Supporting Materials). The bulges disappeared as they approached the tip of the sharp protrusion, leaving only ultrafine pores and pores with setae. For mud crabs, the sharp protrusions of the carapace edge are a specialized defensive function to protect the body from attacks by predators, and the bimodal bulge structure is not necessary in this area.

4.3. Selecting crab samples

Crustaceans grow by molting, so care must be taken when using exoskeletons as research specimens. It is necessary to simultaneously examine not only changes in shell size, which can be observed visually, but also changes in the surface and interior of the hard exoskeleton. It is well known that the exoskeleton of crustaceans such as crabs and shrimp become larger, harder, and thicker through biomineralization over time after molting [50–52]. However, because it is necessary to kill the organism in order to accurately measure the thickness of each layer in the exoskeleton, it is not possible to quantitatively examine the relationship between the time after molting and their thicknesses for one crab. In fact, the results of the exoskeleton thickness shown in Fig. 7 and of the mechanical properties shown in Fig. 8 suggested that the two samples (985 g and 1694 g) did not have a fully formed exoskeleton after molting. Since recently molted crabs contain mostly liquid or a jelly mass with little edible flesh, the method of evaluating hard-shelled crabs is very important for determining the quality of edible crabs. Hence, in addition to carapace color and hardening, there are also methods for evaluating the hardening state of crabs from the sternum of the thoracic appendages [53–55]. These methods can be used as a reference when collecting crab samples.

In Fig. 7, the inner cuticle thickens with growth at $BW = 600$–1000 g. In Okinawa, the crab molts frequently (once every few months) to grow its body until it reaches *BW* 750 g or less. However, when it exceeds 1 kg, it molts once a year. Okinawa crabs hardly molt during the four months of winter, from November to February. During this period, males are thin and mate. Female crabs migrate to the sea to spawn from March to June. Zoea drift in the sea, and crabs that settle in brackish waters (megaloba: May to June) molt repeatedly and become juvenile crabs with $CW = 40$ mm (June to July). After that, they grow larger by molting repeatedly, and they become adult crabs. The area where the endocuticle thickens with *BW*, as shown in Fig. 7, is thought to be strongly related to the molting cycle.

In Fig. 5 and7, the size of the surface bulge and the T_{exo} of the 985 g and 1694 g crabs with thin endocuticles were not significantly different from those of the other crabs. This means that, when the crabs molted, the hard exocuticle forms faster than the soft endocuticle and soon achieves a surface morphology and a steady-state thickness of 150 μm. However, it should be noted that, even if the exocuticle layer is at a steady-state thickness, its mechanical properties are still low because mineralization is not sufficient (Fig. 8). On the other hand, as shown in Fig. 9, unlike the exocuticle, the mechanical properties of the endocuticle were almost the same as those of other crabs. This means that the endocuticle layer adjacent to the cells is thickened by the supply of fully mineralized TPS from the inner surface. In other words, in the exoskeleton after molting, the surface morphology and exocuticle thickness essential for survival are formed first, and then the endocuticle is formed. The endocuticle is thickened by laminating a twisted plywood-pattern layer that is created from the inside surface. While the endocuticle is forming to a thickness corresponding to the body size, the exocuticle is completely hardened by supplying necessary ions and nutrients from inner cells through the pore canal tubules. Yano and

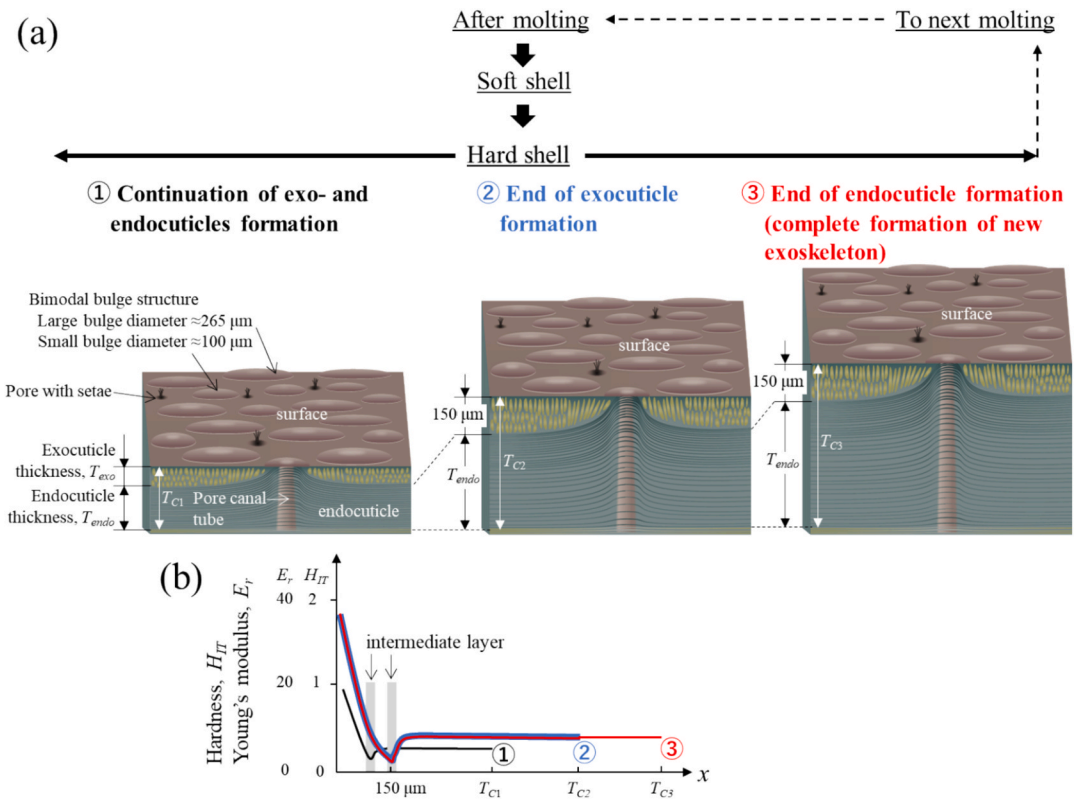

Fig. 10. Schematic diagram of (a) exoskeleton formation and (b) mechanical property change after molting in mud crabs.

Kobayashi [56] investigated the relationship between the number of lamellae in the endocuticle (*NLa*) and the carapace width (*CW*) of 100 shore crabs, *Gaetice depressus*, in the intermolt stage, that live in Hokkaido, Japan. The *NLa* and the total thickness of the endocuticle (T_{endo}) showed a positive correlation, and the *NLa* and T_{endo} increased with the growth of the carapace, irrespective of sex. In this relationship, when the *CW* was small (6–10 mm), the T_{endo} was almost constant (80 μm), and then as the *CW* increased, the *NLa* and T_{endo} increased, and the variation increased. This feature is consistent with the change of T_{endo} against *BW* shown in Fig. 7. The cuticle formation of the hard shell after molting can be summarized as shown in Fig. 10.

As a future issue, it will be necessary to study the relationship between the surface morphology, internal structure, thickness of the exocuticle and endocuticle, and mechanical properties of the robust exoskeleton, including more in-depth modeling and numerical simulation [10,57–59]. In the case of the Bouligand structure parallel to the surface shown in Fig. 6, S7 and S8, even if a crack occurs on the surface or inside the exoskeleton, the crack is unlikely to propagate inward. In addition, the exoskeleton has a composite structure consisting of an exocuticle layer with a hardness gradient and a soft endocuticle layer. This type of tissue structure may provide hints for the development of high-performance materials that will never break. New 3D printing technology enables the production of complex hierarchical structures, replicating the functional and mechanical properties of organisms.

5. Conclusions

This study simultaneously examined shell size and surface morphology and internal changes in the exoskeleton over a wide range of adult mud crab body weights, including the effects of molting. The main results are as follows:

(1) The growth coefficient of mud crabs collected in Okinawa, Japan, were 3.52 for males and 2.91 for females. These values were the largest of those reported so far in Iran, Indonesia, Mozambique, Bangladesh, Oman, and India.
(2) The carapace surface is composed of a bimodal bulge structure, with the diameters of the large and small bulges being 264.5 μm and 100.0 μm, respectively. These bulge sizes are independent of body weight (*BW*).
(3) The exocuticle thickness was constant at approximately 150 μm regardless of *BW*, whereas the endocuticle thickness was approximately 750 μm when $BW < 600$ g, increasing with *BW* in the range of $600 < BW < 1000$ g, and reaching 1200 μm when $BW > 1000$ g.
(4) The hardness (0.3 GPa) and elastic modulus (12.0 GPa) in endocuticle layer are independent of *BW*.
(5) When using crab exoskeletons as research specimens, care must be taken because some specimens do not have a fully formed exoskeleton and their exocuticles are less hard and their endocuticles are thinner than those of normal crab specimens.

CRediT authorship contribution statement

Tadanobu Inoue: Writing – review & editing, Writing – original draft, Visualization, Validation, Supervision, Software, Project administration, Methodology, Investigation, Funding acquisition, Data curation, Conceptualization. **Takahiro Yoshihama:** Writing – review & editing, Resources, Investigation.

Funding

This study was supported by JSPS KAKENHI Grant Number JP21H04537. The grants are greatly appreciated.

Declaration of competing interest

The authors declare that they have no known competing financial

interests or personal relationships that could have appeared to influence the work reported in this paper.

Acknowledgments

We would like to thank M. Sakano for preparing samples, analyzing surface topography, and conducting nanoindentation testing and Y. Kashihara for creating the illustrations.

Appendix A. Supplementary data

Supplementary data to this article can be found online at https://doi.org/10.1016/j.matdes.2025.114699.

Data availability

No data was used for the research described in the article.

References

[1] A.G. Collado, J.M. Blanco, M.K. Gupta, R.D. Vicentea, Advances in polymers based multi-material additive-manufacturing techniques: State-of-art review on properties and applications, Addit. Manuf. 50 (2022) 102577, https://doi.org/10.1016/j.addma.2021.102577.
[2] C. Tung, Y. Chen, W. Chen, P. Chen, Bio-inspired, helically oriented tubular structures with tunable deformability and energy absorption performance under compression, Mater. Des. 222 (2022) 111076, https://doi.org/10.1016/j.matdes.2022.111076.
[3] L. Guan, W. Peng, R. Wen, J. Fan, H. Ferrand, Izod impact resistance of 3D printed discontinuous fibrous composites with Bouligand structure, NPG Asia Mater. 15 (2023) 60, https://doi.org/10.1038/s41427-023-00508-6.
[4] A. Prihar, S. Gupta, H.S. Esmaeeli, R. Moini, Tough double-bouligand architected concrete enabled by robotic additive manufacturing, Nature Comm. 15 (2024) 7498, https://doi.org/10.1038/s41467-024-51640-y.
[5] L. Bai, L. Liu, M. Esquivel, B.L. Tardy, S. Huan, X. Niu, S. Liu, G. Yang, Y. Fan, O. J. Rojas, Nanochitin: chemistry, structure, assembly, and applications, Chem. Rev. 122 (2022) 11604–11674.
[6] S. Chen, S. Wen, S. Zhang, C. Wang, S. Yu, Biological and bioinspired Bouligand structural materials: recent advances and perspectives, Matter 7 (2024) 378–407, https://doi.org/10.1016/j.matt.2023.11.013.
[7] I.M. Meerbeek, J.M. Lenhardt, W. Small, T.M. Bryson, E.B. Duoss, T.H. Weisgraber, Compressive properties of silicone Bouligand structures, MRS Bull. 48 (2023) 325–331, https://doi.org/10.1557/s43577-022-00398-z.
[8] Y. Tang, C. Liu, R. Xiong, Biomimetic mechanically robust chiroptical hydrogel enabled by hierarchical bouligand structure engineering, ACS Nano 18 (2024) 14629–14639, https://doi.org/10.1021/acsnano.4c02677.
[9] Y. Bouligand, Twisted fibrous arrangements in biological materials and cholesteric mesophases, Tissue Cell 4 (1972) 189–217, https://doi.org/10.1016/S0040-8166(72)80042-9.
[10] W. Lin, P. Liu, S. Li, J. Tian, W. Cai, X. Zhang, J. Peng, C. Miao, H. Zhang, P. Gu, Z. Wang, Z. Zhang, T. Lu, Multi-scale design of the chela of the hermit crab *Coenobita brevimanus*, Acta Biomater. 127 (2021) 229–241, https://doi.org/10.1016/j.actbio.2021.04.012.
[11] H.-O. Fabritius, E.S. Karsten, K. Balasundaram, S. Hild, K. Huemer, D. Raabe, Correlation of structure, composition and local mechanical properties in the dorsal carapace of the edible crab Cancer pagurus, Z, Kristallogr 227 (2012) 766–776, https://doi.org/10.1524/zkri.2012.1532.
[12] H.-O. Fabritius, C. Sachs, P.R. Triguero, D. Raabe, Influence of structural principles on the mechanics of a biological fiber-based composite material with hierarchical organization: the exoskeleton of the lobster homarus americanus, Adv. Mater. 21 (2009) 391–400, https://doi.org/10.1002/adma.200801219.
[13] T. Inoue, T. Hiroto, Y. Hara, K. Nakazato, S. Oka, Tissue structure and mechanical properties of the exoskeleton of the huge claws of the mud crab, *Scylla serrata*, J. Mater. Sci. 58 (2023) 1099–1115, https://doi.org/10.1007/s10853-022-08083-x.
[14] D. Raabe, C. Sachs, P. Romano, The crustacean exoskeleton as an example of a structurally and mechanically graded biological nanocomposite material, Acta Mater. 53 (2005) 4281–4292, https://doi.org/10.1016/j.actamat.2005.05.027.
[15] R. Rose, R. Dillaman, The structure and calcification of the crustacean cuticle, Am. Zool. 24 (1984) 893–909, https://doi.org/10.1093/icb/24.4.893.
[16] T. Inoue, S. Oka, T. Hara, Three-dimensional microstructure of robust claw of coconut crab, one of the largest terrestrial crustaceans, Mater. Des. 206 (2021) 109765, https://doi.org/10.1016/j.matdes.2021.109765.
[17] T. Inoue, T. Hara, K. Nakazato, S. Oka, Superior mechanical resistance in the exoskeleton of the coconut crab, *Birgus latro*, Mater. Today Bio. 12 (2021) 100132, https://doi.org/10.1016/j.mtbio.2021.100132.
[18] M. Vittori, V. Srot, L. Korat, M. Rejec, P. Sedmak, B. Bussmann, F. Predel, P. A. Aken, J. Štrus, The mechanical consequences of the interplay of mineral distribution and organic matrix orientation in the claws of the sea slater *Ligia pallasii*, Minerals 11 (2021) 1373, https://doi.org/10.3390/min11121373.
[19] Y. Wang, X. Li, J. Li, F. Qiu, Microstructure and mechanical properties of the dactylopodites of the chinese mitten crab (*Eriocheir sinensis*), Appl. Sci. 8 (2018) 674, https://doi.org/10.3390/app8050674.
[20] I. Kellersztein, S.R. Cohen, B. Bar-On, H.D. Wagner, The exoskeleton of scorpions' pincers: structure and micro-mechanical properties, Acta Biomater. 94 (2019) 565–573, https://doi.org/10.1016/j.actbio.2019.06.036.
[21] F. Nekvapil, S.C. Pinzaru, L. Barbu-Tudoran, M. Suciu, B. Glamuzina, T. Tamaș, V. Chiș, Color-specific porosity in double pigmented natural 3d-nanoarchitectures of blue crab shell, Sci. Rep. 10 (2020) 3019.
[22] A.Z. Qian, M. Yang, L. Zhou, J. Liu, R. Akhtar, C. Liu, Y. Liu, L. Ren, L. Ren, Structure, mechanical properties and surface morphology of the snapping shrimp claw, J. Mater. Sci. 53 (2018) 10666–10678, https://doi.org/10.1007/s10853-018-2364-7.
[23] T. Inoue, S. Oka, K. Nakazato, T. Hara, Structural changes and mechanical resistance of claws and denticles in coconut crabs of different sizes, Biology 10 (2021) 1304, https://doi.org/10.3390/biology10121304.
[24] T. Inoue, Y. Hara, K. Nakazato, Mechanical resistance of the largest denticle on the movable claw of the mud crab, Biomimetics 8 (2023) 602, https://doi.org/10.3390/biomimetics8080602.
[25] T. Inoue, S. Oka, T. Hiroto, Mechanical properties tissue structure, and elemental composition of the walking leg tips of coconut crabs, J. Mar. Sci. Eng. 12 (2024) 639, https://doi.org/10.3390/jmse12040639.
[26] B.W. Cribb, A. Rathmell, R. Charters, R. Rasch, H. Huang, I.R. Tibbetts, Structure, composition and properties of naturally occurring non-calcified crustacean cuticle, Arthropod. Struct. Dev. 38 (2009) 173–178, https://doi.org/10.1016/j.asd.2008.11.002.
[27] H. Alberts-Hubatsch, S.Y. Lee, J.-O. Meynecke, K. Diele, I. Nordhaus, M. Wolff, Life-history, movement, and habitat use of *scylla serrata* (decapoda, portunidae): current knowledge and future challenges, Hydrobiologia 763 (2015) 5–21, https://doi.org/10.1007/s10750-015-2393-z.
[28] H. Khaksari, M. Safaie, A. Salarzadeh, Population dynamics and reproductive biology of *Scylla serrata* (Forskal, 1775) on the shores overlooking the mangrove forest of the Persian Gulf, Reg. Stud. Mar. Sci. 57 (2023) 102758, https://doi.org/10.1016/j.rsma.2022.102758.
[29] A. Mohapatra, R.K. Mohanty, S.K. Mohanty, S.K. Dey, Carapace width and weight relationships, condition factor, relative condition factor and gonado-somatic index (GSI) of mud crabs (*Scylla spp.*) from Chilika Lagoon India, Indian J. Mar. Sci. 39 (2010) 120.
[30] B. Widigdo, R. Rukisah, A. Laga, A. Hakim, Y. Wardiatno, Carapace length-weight and width-weight relationships of *Scylla serrata* in Bulungan District North Kalimantan, Indonesia, Biodiversitas. 18 (2017) 1316, https://doi.org/10.20950/10.13057/biodiv/d180405.
[31] S. Toivio, Size, sex and distribution of *Scylla serrata* on Inhaca Island, Mozambique. [Thesis]. (2015) University of Gothenburg, Gothenburg, Sweden.
[32] D.A. Waugh, R.M. Feldmann, A.M. Schroeder, M.H. Mutel, Differential cuticle architecture and its preservation in fossil and extant Callinectes and *Scylla* claws, J. Crustacean Biol. 26 (2006) 271–282, https://doi.org/10.1651/S-2692.1.
[33] Fisheries Fact Sheet (Mud Crab). 2013. Available online: https://marinewaters.fish.wa.gov.au/mwwp/wp-content/uploads/2019/06/CR530-Fisheries-Fact-Sheet-28-Mud-Crab-WEB.pdf (accessed on 18 August 2025).
[34] T. Inoue, Y. Hara, K. Nakazato, Mechanical resistance and tissue structure of claw denticles of various sizes in the mud crab Scylla Serrata, Materials 16 (2023) 4114, https://doi.org/10.3390/ma16114114.
[35] T. Inoue, Q. Hai, K. Nakazato, Reliability of the Young's modulus of crab exoskeleton materials estimated from nanoindentation tests, J. Mater. Res. Technol. 33 (2024) 2210–2215, https://doi.org/10.1016/j.jmrt.2024.09.194.
[36] T. Inoue, E. Kitahara, Y. Hara, K. Nakazato, Mud club's mottled, deep-blue exoskeleton: surface morphology and internal microstructure, Minerals 12 (2022) 1607, https://doi.org/10.3390/min12121607.
[37] H. Triajie, S. Andayani, U. Yanuhar, A.W. Ekawati, Structure of hard and soft carapace exoskeleton biomaterial through SEM-EDXRS at various stages of development *Scylla paramamosain* Mud Crab, Int. Biology Biomedical Eng. 15 (2021) 113, https://doi.org/10.46300/91011.2021.15.15.
[38] S.C. Schenk, P.C. Wainwright, Dimorphism and the functional basis of claw strength in six brachyuran crabs, J. Zool. 255 (2001) 105–119, https://doi.org/10.1017/S0952836901001157.
[39] A.A. Kumalah, Y. Wardiatno, I. Setyobudiandi, A. Fahrudin, Population Biology of mud crab Scylla serrata - Forsskal, 1775 in Mangrove Ecosystem of Subang District, West Java, J. Technol. Kelautan Topics. 9 (2017) 173–184.
[40] M.Y. Ali, D. Kamal, S.M.M. Hossain, M.A. Azam, W. Sabbir, A. Murshida, B. Ahmed, K. Azam, Biology studies of the mud crab, *Scylla serrate* (Forskal) of the Sundarbans Mangrove Ecosystem in Khulna Region of Bangladesh, Pakistan, J. Biol. Sci. 7 (2004) 1981–1987. https://scialert.net/abstract/?doi=pjbs.2004.1981.1987.
[41] R. Savari, R. Naderloo, E. Kamrami, M.R. Atagholipour, Preliminary biological information of *Scylla serrata* (Forskål, 1775) (Brachyura, Portunidae) in the Persian Gulf and Gulf of Oman: a conservation priority, Crustaceana 86 (2013) 322–335, https://doi.org/10.1163/15685403-00003174.
[42] K.A. Aneesa, E.R. Chaithanya, S.P. Varghese, Biometric indices of *Scylla serrata* (Forskal, 1775): exploring gender-specific growth patterns from the Cochin Estuary, southwest coast of India, Heliyon 11 (2025) e42829, https://doi.org/10.1016/j.heliyon.2025.e42829.
[43] Y. Ikeda, H. Ozaki, H. Yasuda, Growth of sclaes in goldfish, Bull. Japan. Soc. Sci. Fisheries 39 (1973) 25–33, https://doi.org/10.2331/suisan.39.25.

[44] G.P. Busacker, I.R. Adelman, E.M. Goolish, Ch.11 Growth, Methods for Fish Biology, in: C.B.Schreck, P.B.Moyle (Eds.), (1990) Ameican fisheries society, USA, pp.363-387.
[45] L. Wen, J.C. Weaver, G.V. Lauder, Biomimetic shark skin: design, fabrication and hydrodynamic function, J. Exper. Biol. 217 (2014) 1656–1666, https://doi.org/10.1242/jeb.097097.
[46] H.A. Abdulbari, H.D. Mahammed, Z.B.Y. Hassan, Bio-inspired passive drag reduction techniques: a review, Chem. Bio. Eng. 2 (2015) 183–203, https://doi.org/10.1002/cben.201400033.
[47] S. Nishimoto, B. Bhushan, Bioinspired self-cleaning surfaces with superhydrophobicity, superoleophobicity, and superhydrophilicity, RSC Adv. 3 (2013) 671–690, https://doi.org/10.1039/C2RA21260A.
[48] T. Darmanin, F. Guittard, Superhydrophobic and superoleophobic properties in nature, Mater. Today 18 (2015) 273–285, https://doi.org/10.1016/j.mattod.2015.01.001.
[49] W. Barthlott, M. Mail, B. Bhushan, K. Koch, Plant surfaces: structures and functions for biomimetic innovations, Nano-Micro Lett. 9 (2017) 1265–1305, https://doi.org/10.1007/s40820-016-0125-1.
[50] The Biology and Management of Lobsters: Vol. I: Physiology and Behavior, in: J. Stanley, B.F. Phillips (Eds.), (1980), Academic Press Inc., New York.
[51] J. Salaenoi, J. Bootpugdeethum, M. Mingmuang, A. Thongpan, Variation of Calcium N-acetylglucosamine, Glucosamine and Glucose Content during Molting Cycle of Mud Crab (*Scylla serrata* Forskal 1775), Kasetsart J. (Nat. Sci.) 40 (2006) 668–679, accessed on 10 January 2025, https://www.thaiscience.info/journals/Article/TKJN/10471318.pdf.
[52] J.N. Cameron, Post-molt calcification in the blue crab, Callinectes sapidus – timing and mechanism, J. Exp. Biol. 143 (1989) 285–304, https://doi.org/10.1242/jeb.143.1.285.
[53] S.L. Kurkute, A.S. Pawase, S. Dey, D.I. Pathan, M.S. Sawant, S. Swain, Effect of some minerals on shell hardening of mud crab, *Scylla serrata* (Forskal, 1775), Int. J. Fish. Aquatic Stud. 7 (2017) 44–47, accessed on 16 January 2025, https://www.fisheriesjournal.com/archives/2019/vol7issue1/PartA/7-1-10-534.pdf.
[54] How to check if your Mud Crab is FULL or EMPTY with Mal, Adam Kilpatrick Fishing, (2024) https://www.youtube.com/watch?v=cdGZASCtFFc. (accessed on 10 January 2025).
[55] L. Towers, How to Check if Your Mud Crab is Full of Meat, The fish site (2015). https://thefishsite.com/articles/how-to-check-if-your-mud-crab-is-full-of-meat (accessed on 10 January 2025).
[56] I. Yano, S. Kobayashi, Calcification and age determination in crustacea-‡I. possibility of age determination in crabs on the basis of number of lamellae in cuticles, Bull. Japan. Soc. Sci. Fisheries 35 (1969) 34–42, https://doi.org/10.2331/suisan.35.34.
[57] Z. Zhang, Y. Zhang, H. Gao, On optimal hierarchy of load-bearing biological materials, Proc. Royal Soc. B: Biol. Sci. 278 (2011) 519–525, https://doi.org/10.1098/rspb.2010.1093.
[58] H. Li, K. Geng, B. Zhu, Q. Zhang, Y. Wen, Z. Zhang, Y. Yuan, H. Gao, Mineral asperities reinforce nacre through interlocking and friction-like sliding, J. Mech. Phys. Solids 190 (2024) 105712, https://doi.org/10.1016/j.jmps.2024.105712.
[59] T. Inoue, M. Iwai, Pinching simulation of the coconut crab considering the 3D shape and internal characteristics of the robust claw exoskeleton, Results in Eng. 27 (2025), https://doi.org/10.1016/j.rineng.2025.10572.